

## Supplementary Information

### Rapid SARS-CoV-2 Detection by Carbon Nanotube-Based Near-Infrared Nanosensors

Rebecca L. Pinals,<sup>1</sup> Francis Ledesma,<sup>1</sup> Darwin Yang,<sup>1</sup> Nicole Navarro,<sup>2</sup> Sanghwa Jeong,<sup>1</sup> John E. Pak,<sup>3</sup> Lili Kuo,<sup>4</sup> Yung-Chun Chuang,<sup>5,6</sup> Yu-Wei Cheng,<sup>5</sup> Hung-Yu Sun,<sup>7</sup> Markita P. Landry\*<sup>1,3,8,9</sup>

<sup>1</sup> Department of Chemical and Biomolecular Engineering, University of California, Berkeley, California 94720, United States

<sup>2</sup> Department of Chemistry, University of California, Berkeley, California 94720, United States

<sup>3</sup> Chan-Zuckerberg Biohub, San Francisco, California 94158, United States

<sup>4</sup> Wadsworth Center, New York State Department of Health, Slingerlands, New York 12159, United States

<sup>5</sup> Leadgene Biomedical Inc., Tainan 71042, Taiwan

<sup>6</sup> Department of Medical Laboratory Science and Biotechnology, College of Medicine, National Cheng Kung University, Tainan 70101, Taiwan

<sup>7</sup> Institute of Molecular Medicine, College of Medicine, National Cheng Kung University, Tainan 70101, Taiwan

<sup>8</sup> Innovative Genomics Institute (IGI), Berkeley, California 94720, United States

<sup>9</sup> California Institute for Quantitative Biosciences, QB3, University of California, Berkeley, California 94720, United States

The ratio of ACE2 to  $(GT)_6$ -SWCNTs was chosen based on a protein footprint estimation that 28.6 ACE2 dimers fit per SWCNT in the close-packed limit (using ACE2 dimer dimensions as determined by cryo-EM (1)). This calculation translates to a mass ratio of 2.36 ACE2:SWCNT. The actual mass ratio of 2.5 ACE2:SWCNT was chosen to be just above this theoretical close-packed limit in an attempt to minimize protein spreading that arises from a large excess of nanoparticle surface available for proteins. Extending to twice this mass ratio produces more quenching in the SWCNT fluorescence (**Figure S1**), yet reduced sensing ability (**Figure S2**) and colloidal stability. Thus, the mass ratio of 2.5 ACE2:SWCNT was experimentally determined to be best suited for S RBD sensing (**Figure S2**).

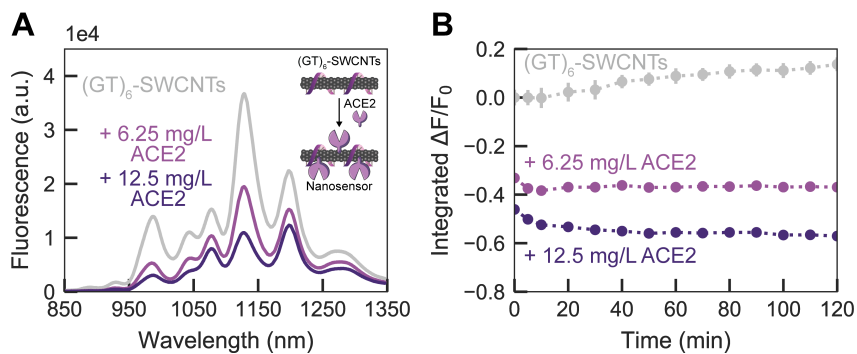


**Figure S1. Adsorption of different ratios of ACE2 on  $(GT)_6$ -SWCNTs.** ACE2-SWCNT complexation quenched intrinsic SWCNT near-infrared fluorescence, shown by **(A)** the full fluorescence spectrum after 1 h incubation of 6.25 mg/L or 12.5 mg/L ACE2 with 2.5 mg/L  $(GT)_6$ -SWCNTs (final concentrations) and **(B)** the integrated-fluorescence change as a function of time over 2 h. Both ratios exhibit stable quenched fluorescence, however, the lower ratio of protein to SWCNT exhibited better colloidal stability.

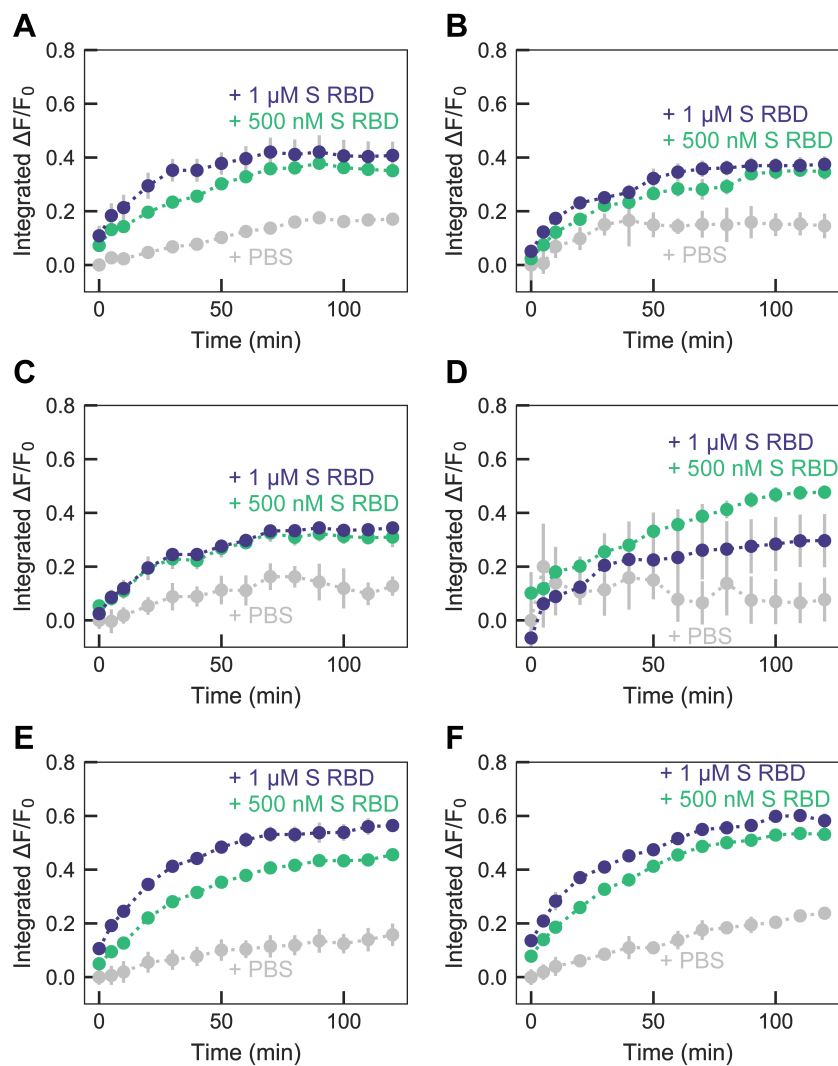


**Figure S2. Response of different ratios ACE2:(GT)<sub>6</sub>-SWCNTs to S RBD.** Integrated-fluorescence fold change as a function of time over 120 min upon addition of PBS, 500 nM S RBD, or 1  $\mu$ M S RBD to nanosensor formed by (A) 6.25 mg/L ACE2 and 2.5 mg/L (GT)<sub>6</sub>-SWCNTs incubated 1 h, (B) 12.5 mg/L ACE2 and 2.5 mg/L (GT)<sub>6</sub>-SWCNTs incubated 1 h, (C) 6.25 mg/L ACE2 and 2.5 mg/L (GT)<sub>6</sub>-SWCNTs incubated 3 h, (D) 12.5 mg/L ACE2 and 2.5 mg/L (GT)<sub>6</sub>-SWCNTs incubated 3 h, (E) 6.25 mg/L ACE2 and 2.5 mg/L (GT)<sub>6</sub>-SWCNTs incubated 30 min, diluted by half in PBS, and incubated an additional 30 min, and (F) 12.5 mg/L ACE2 and 2.5 mg/L (GT)<sub>6</sub>-SWCNTs incubated 30 min, diluted by half in PBS, and incubated an additional 30 min.

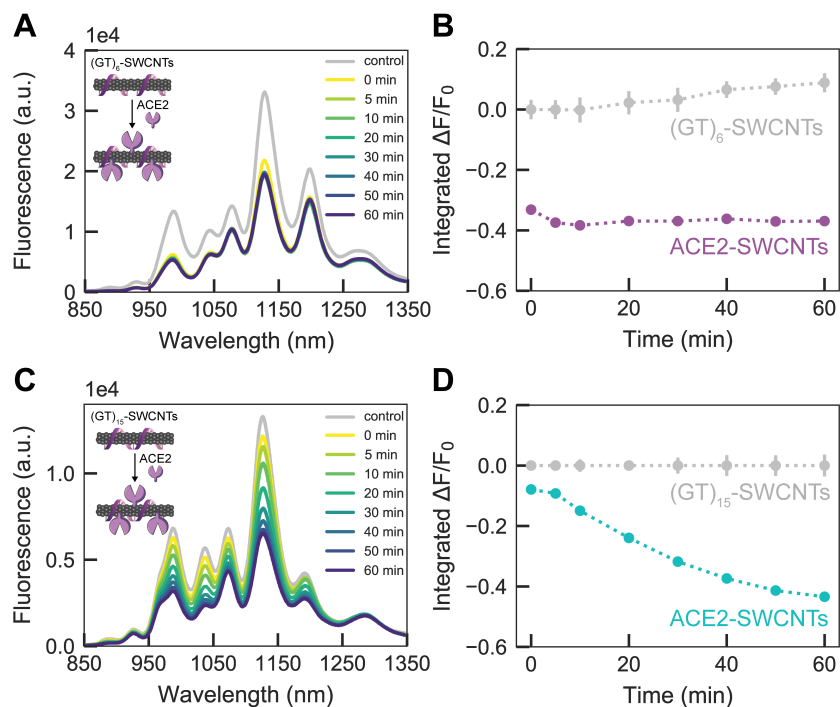


**Figure S3. Adsorption of ACE2 to  $(GT)_6$ - vs.  $(GT)_{15}$ -SWCNTs.** ACE2-SWCNT complexation rapidly quenched intrinsic SWCNT near-infrared fluorescence, shown by **(A)** the full fluorescence spectrum and **(B)** the integrated-fluorescence fold change as a function of time over 1 h, upon incubation of 6.25 mg/L ACE2 with 2.5 mg/L  $(GT)_6$ -SWCNTs (final concentrations). ACE2-SWCNT complexation quenched intrinsic SWCNT near-infrared fluorescence at a slower rate, shown by **(C)** the full fluorescence spectrum and **(D)** the integrated-fluorescence fold change as a function of time over 1 h, upon incubation of 6.25 mg/L ACE2 with 2.5 mg/L  $(GT)_{15}$ -SWCNTs (final concentrations).

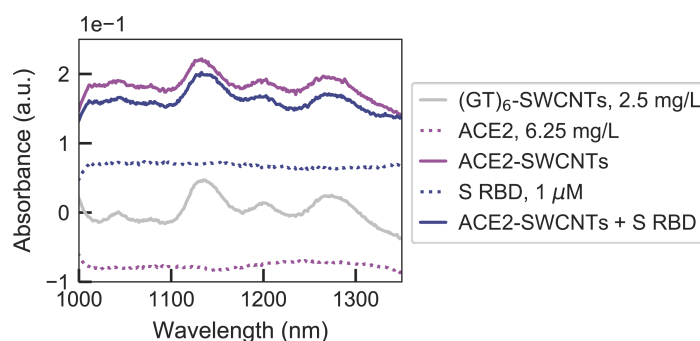


**Figure S4. Absorbance of  $(GT)_6$ -SWCNTs with ACE2 sensing protein and S RBD analyte.** Retention of near-infrared absorbance peaks arising from SWCNT in the case of ACE2 adsorption and S RBD analyte binding confirms the noncovalent passivation, rather than covalent modification, of the SWCNT surface.

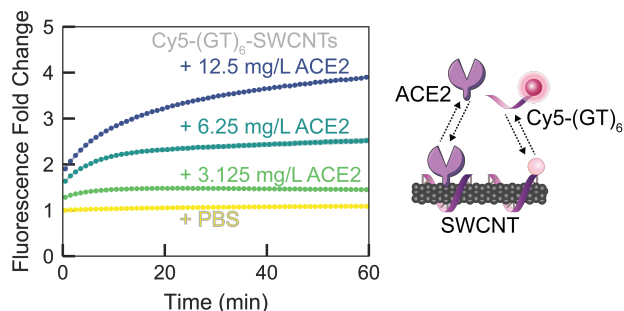


**Figure S5. Displacement of Cy5-(GT)<sub>6</sub> ssDNA from SWCNT as a function of passivating ACE2 concentration.** Adsorption of ACE2 on the SWCNT surface led to (GT)<sub>6</sub> desorption, tracked by Cy5-labeled ssDNA, in a concentration-dependent manner upon addition of varying ACE2 concentrations with 2.5 mg/L Cy5-(GT)<sub>6</sub>-SWCNTs (final concentrations). The increase in Cy5-(GT)<sub>6</sub> fluorescence from the initial quenched state on the SWCNT serves as a proxy for ACE2 adsorption. Shaded error bars represent standard error between experimental replicates (N = 3).

To test the stability of the ACE2-functionalized SWCNT construct, we implemented a solvatochromic shift assay (2, 3). This methodology is based upon addition of surfactant (sodium cholate, SC) that coats any solvent-exposed SWCNT surface and can displace low-affinity molecules from the SWCNT surface. SC adsorption causes exclusion of water from the SWCNT surface, producing a large increase in fluorescence and solvatochromic shift to lower emission wavelengths. Prior to ACE2 incubation, SC elicited both a large blue-shift (-16 nm) and sizeable increase in fluorescence (70.2%) for (GT)<sub>6</sub>-SWCNTs alone (**Figure S6A-B**). However, upon passivation with ACE2, these spectral changes were reduced to -10 nm and 10.3%, respectively (**Figure S6C-D**), suggesting a mechanism in which ACE2 adsorbs to the SWCNT surface and causes (GT)<sub>6</sub> ssDNA desorption. Moreover, we show that addition of S RBD analyte to the ACE2-SWCNT complex further stabilizes the nanosensor, whereby addition of SC produced a brief blue-shift of -6 nm yet a complete return to baseline by 70 min, and similarly, a minimal change in fluorescence of -3.9% (**Figure S6E-F**).

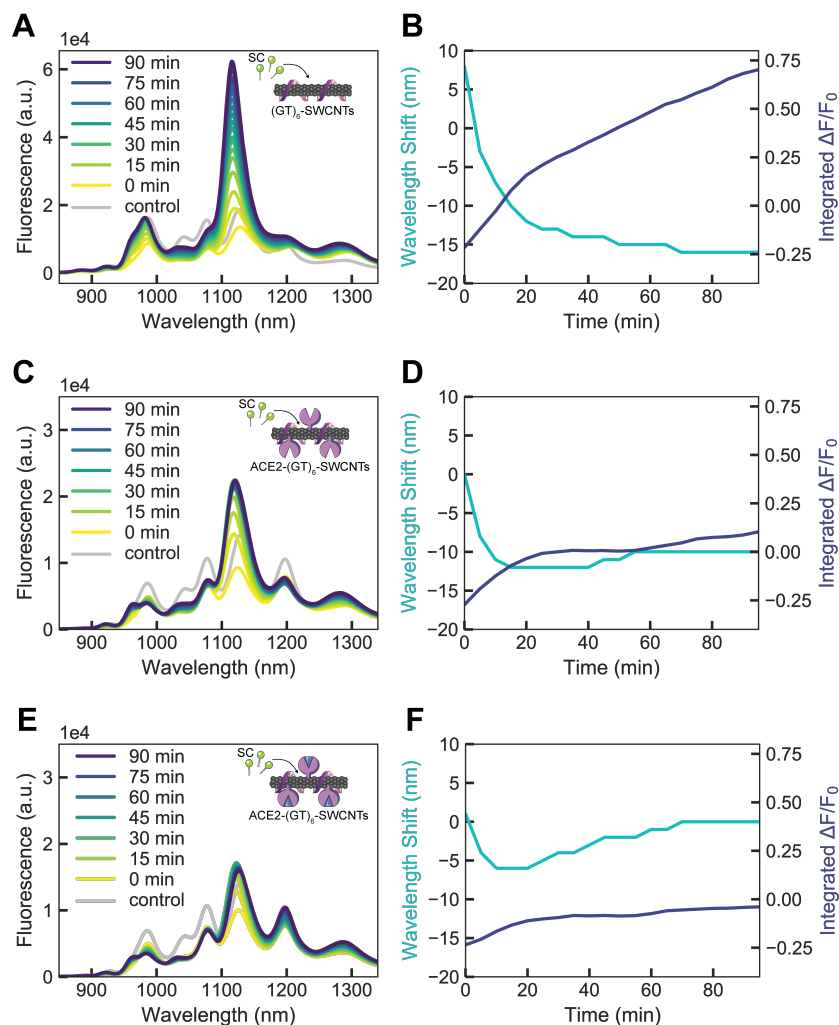


**Figure S6. Surfactant displacement experiment to probe the stability of  $(GT)_6$ -SWCNTs with ACE2 sensing protein and S RBD analyte.** Full fluorescence spectrum (left) and time-dependent wavelength shift and integrated-fluorescence fold change (right) for **(A-B)** 2.5 mg/L  $(GT)_6$ -SWCNTs alone, **(C-D)** ACE2-SWCNT nanosensors (formed by 6.25 mg/L ACE2 and 2.5 mg/L  $(GT)_6$ -SWCNTs), and **(E-F)** ACE2-SWCNT nanosensors with 500 nM S RBD, each upon addition of 0.25 w/v% sodium cholate (SC, final concentration). Decreasing blue-shift and fluorescence fold change due to ACE2 implies ACE2 covers and stabilizes the SWCNT surface, with further stabilization upon addition of S RBD analyte.

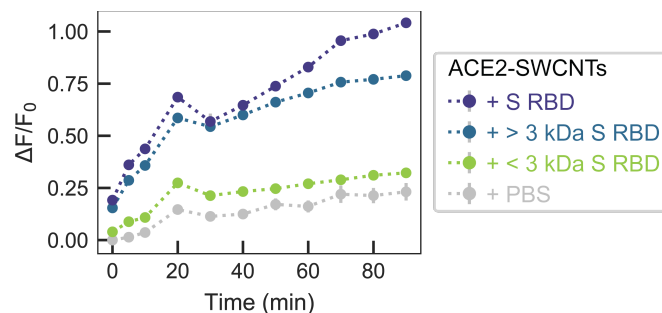


**Figure S7. ACE2-SWCNT nanosensor response to controls.** Addition of 500 nM S RBD (final concentration) to ACE2-SWCNTs (formed by 6.25 mg/L ACE2 and 2.5 mg/L (GT)<sub>6</sub>-SWCNTs) yielded a significant turn-on fluorescence response. This response is maintained for S RBD > 3 kDa MWCO centrifugal filter and absent for S RBD < 3 kDa.

The limit of detection (*LOD*) of the ACE2-SWNT nanosensor for S RBD analyte is defined as the lowest analyte concentration likely to be reliably distinguished from the limit of blank (*LOB*) (4). The *LOB* is the highest apparent analyte concentration expected to be found when replicates of a blank sample containing only buffer (no analyte) are tested:

$$LOB = mean_{blank} + 1.645 SE_{blank}$$

Where the mean and standard error (*SE*) are in terms of the fluorescence fold change ( $\Delta F/F_0$ ). For the concentration series of S RBD analyte tested (**Figure 2D-E**), the *LOB* is calculated to be  $\Delta F/F_0 = 0.2828$ . The limit of detection is then:

$$LOD = LOB + 1.645 SE_{low\ conc.}$$

Where the low concentration is set as the fluorescence values corresponding to 50 nM S RBD. Thus, the *LOD* is calculated to be  $\Delta F/F_0 = 0.2919$ , which corresponds to a S RBD concentration of 9.49 nM based on the cooperative binding model fit.

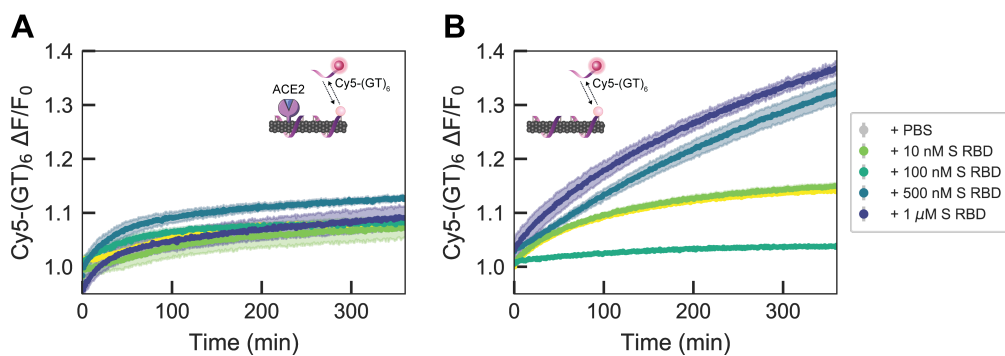


**Figure S8. Displacement of Cy5-(GT)<sub>6</sub> ssDNA from SWCNT in the presence or absence of ACE2 sensing protein, as a function of S RBD analyte concentration.** Addition of varying concentrations of S RBD analyte to **(A)** ACE2-Cy5-(GT)<sub>6</sub>-SWCNT nanosensors (formed by 6.25 mg/L ACE2 and 2.5 mg/L (GT)<sub>6</sub>-SWCNTs) and **(B)** Cy5-(GT)<sub>6</sub>-SWCNTs alone (2.5 mg/L). Shaded error bars represent standard error between experimental replicates (N = 3).



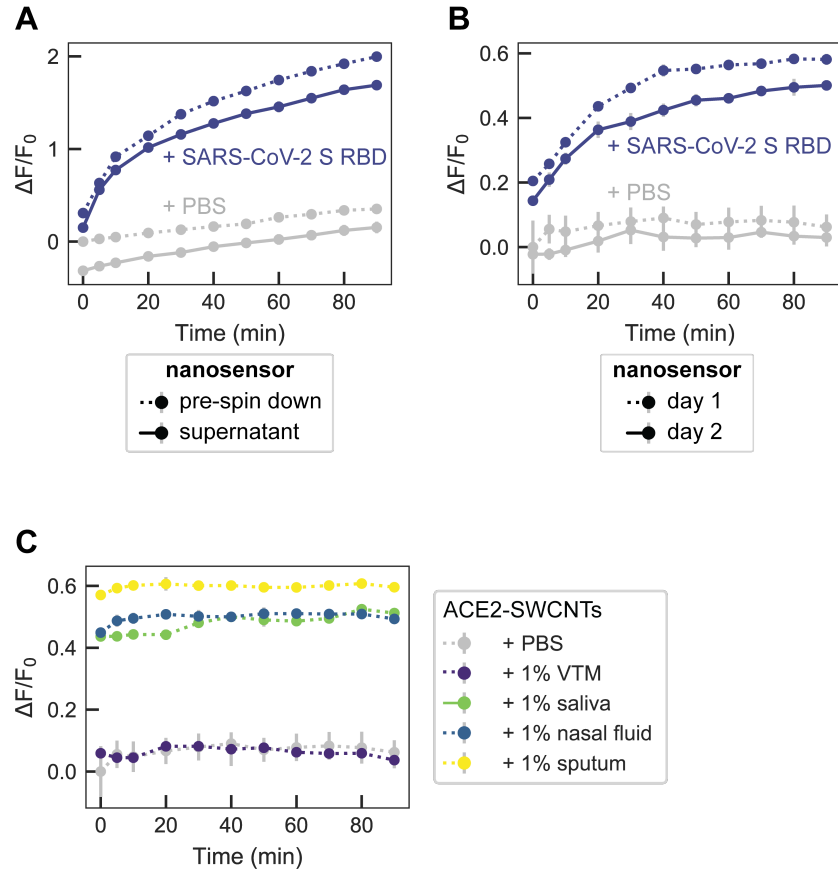


**Figure S9. ACE2-SWCNT nanosensor controls for assessing stability.** Response of ACE2-SWCNTs (formed by 6.25 mg/L ACE2 and 2.5 mg/L (GT)<sub>6</sub>-SWCNTs) to S RBD was preserved **(A)** before and after centrifugation (16.1 krcf, 30 min; 500 nM S RBD) and **(B)** before and after overnight incubation at ambient conditions (1  $\mu$ M S RBD). **(C)** Stability of ACE2-SWCNT nanosensors in different biofluids. Normalized change in fluorescence of the 1130 nm SWCNT emission peak for the ACE2-SWCNT sensor as a function of time in 1% relevant biofluids: viral transport medium (VTM), saliva, nasal fluid, and sputum (treated with sputasol). Nanosensor fluorescence in biofluids demonstrated stability yet elevated magnitudes.

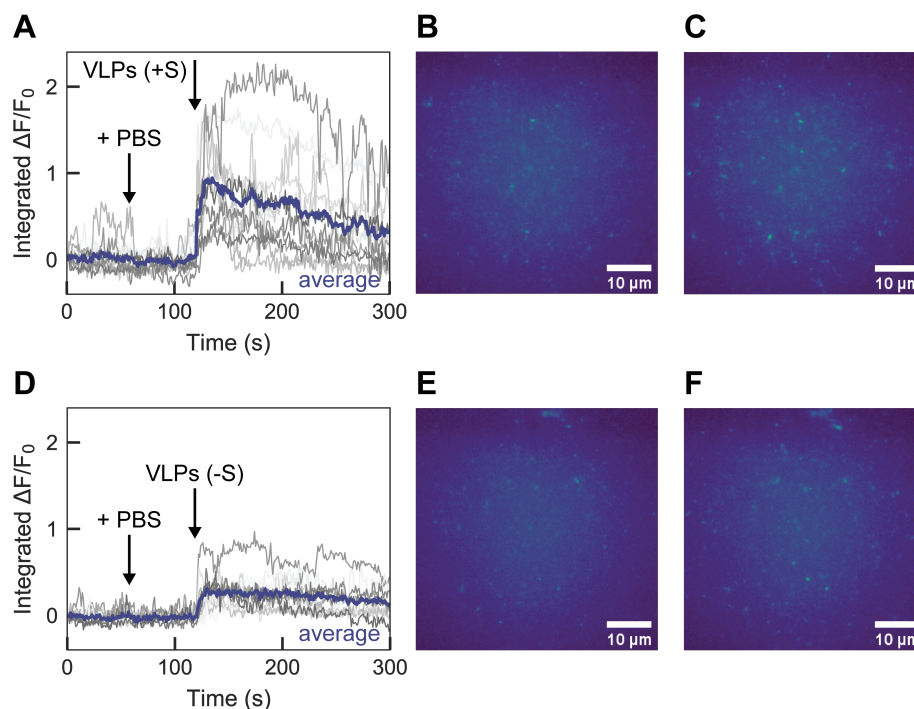


**Figure S10. Surface-immobilized ACE2-SWCNT nanosensor response to virus-like particles (VLPs) with and without S protein.** Single-molecule microscopy traces of ACE2-SWCNTs (formed by 12.5 mg/L ACE2 and 5 mg/L (GT)<sub>6</sub>-SWCNTs) immobilized on a glass microwell dish exhibited a larger fluorescence response to VLPs expressing S protein, for single regions of interest (gray; 12 total per image) and the average intensity (purple). **(A-C)** Addition of PBS at 60 s caused no change in fluorescence, as expected, and addition of 50 mg/L VLPs (no S protein) at 120 s yielded a minor turn-on fluorescence response, as shown by **(A)** the integrated-fluorescence fold change ( $\Delta F/F_0$ ) over 5 min and entire field-of-view at **(B)** time = 100 s and **(C)** time = 125 s. **(D-F)** Addition of PBS at 60 s caused no change in fluorescence, as expected, and addition of 50 mg/L VLPs (with S protein) at 120 s yielded a large turn-on fluorescence response, as shown by **(D)** the integrated-fluorescence fold change ( $\Delta F/F_0$ ) over 5 min and entire field-of-view at **(E)** time = 100 s and **(F)** time = 125 s. All fluorescence images were obtained with 721 nm laser excitation and a 100x oil immersion objective.

This platform for nanosensor design was expanded to attempt passivation of (GT)<sub>6</sub>-SWCNTs with an antibody for SARS-CoV-1 S RBD that has been previously verified to bind CoV-2 S RBD (5). Interestingly, the anti-S sensing protein did not exhibit any modulation in intrinsic SWCNT fluorescence, nor did addition of the S RBD analyte provoke a fluorescence response. This result implying a lack of interaction between anti-S and the SWCNT surface is in line with our previous work that implies antibodies exhibit minimal adsorption to ssDNA-SWCNTs (6). Thus, alternative attachment strategies must be pursued for sensing proteins with no intrinsic affinity for the SWCNT surface.

**Table S1.** Purchased biofluid and protein specifications.

Purpose	Protein	Manufacturer	Lot #	Source	Form	Concentration
Sensing protein	Angiotensin-converting enzyme 2 (ACE2)	Ray Biotech	04U24020GC	Recombinant, (HEK293 cell expression system; C-terminal His-tag)	Liquid (PBS)	2.8 g/L
Control	SARS CoV-1 spike protein receptor-binding domain (CoV-1 S RBD)	ACROBiosystems	3558c-203KF1-R7	Recombinant (HEK293 cell expression system; C-terminal His-tag)	Lyophilized from PBS, 10% Trehalose	Reconstituted in 167 $\mu$ L 0.1 M PBS, 30 min at room temperature with occasional gentle mixing
Control	MERS spike protein receptor-binding domain (MERS S RBD)	MyBioSource	0110YB	Recombinant (HEK293 cell expression system; C-terminal His-tag)	Liquid (PBS, 0.1% sodium azide)	1 g/L
Control	Influenza hemagglutinin subunit (FLU HA1)	MyBioSource	95-101-1104	Recombinant (E. coli expression; N-terminal His-tag and strepII-tag)	Liquid (PBS, 0.1% SDS, 0.02% sodium azide)	1 g/L
Control	Human serum albumin (HSA)	Sigma-Aldrich	#SLBZ2785	Human plasma	Lyophilized, fatty acid and globulin free	Reconstituted in 0.1 M PBS, 30 min at room temperature with occasional gentle mixing
Biofluid	Viral transport medium	Innovative Research	31975	N/A	Liquid	N/A
Biofluid	Saliva	Lee Biosolutions	W205820	Human, pooled, normal	Liquid	N/A
Biofluid	Nasal fluid	Lee Biosolutions	18-05-538	Human, single donor, normal	Liquid	N/A
Biofluid	Sputum	Lee Biosolutions	18-03-594	Human, single donor, normal	Liquid	N/A

## References

1. R. Yan, Y. Zhang, Y. Li, L. Xia, Y. Guo, Q. Zhou, Structural basis for the recognition of SARS-CoV-2 by full-length human ACE2. *Science*. **367**, 1444–1448 (2020).
2. A. A. Alizadehmojarad, X. Zhou, A. G. Beyene, K. E. Chacon, Y. Sung, R. L. Pinals, M. P. Landry, L. Vuković, Binding Affinity and Conformational Preferences Influence Kinetic Stability of Short Oligonucleotides on Carbon Nanotubes. *Advanced Materials Interfaces*. **7**, 2000353 (2020).
3. A. G. Beyene, A. A. Alizadehmojarad, G. Dorhac, N. Goh, A. M. Streets, P. Král, L. Vuković, M. P. Landry, Ultralarge Modulation of Fluorescence by Neuromodulators in Carbon Nanotubes Functionalized with Self-Assembled Oligonucleotide Rings. *Nano Lett.* **18**, 6995–7003 (2018).

4. D. A. Armbruster, T. Pry, Limit of Blank, Limit of Detection and Limit of Quantitation. *Clin Biochem Rev.* **29**, S49–S52 (2008).
5. M. Yuan, N. C. Wu, X. Zhu, C.-C. D. Lee, R. T. Y. So, H. Lv, C. K. P. Mok, I. A. Wilson, A highly conserved cryptic epitope in the receptor binding domains of SARS-CoV-2 and SARS-CoV. *Science.* **368**, 630–633 (2020).
6. R. L. Pinals, D. Yang, D. J. Rosenberg, T. Chaudhary, A. R. Crothers, A. T. Iavarone, M. Hammel, M. P. Landry, Quantitative Protein Corona Composition and Dynamics on Carbon Nanotubes in Biological Environments. *Angewandte Chemie International Edition* (2020), doi:10.1002/anie.202008175.